THE JOURNAL OF PHYSICAL CHEMISTRY B

Article

pubs.acs.org/JPCB

The Role of Site-Specific Hydrogen Bonding Interactions in the Solvation Dynamics of *N*-Acetyltryptophanamide

Fabrizio Messina,[†] Ahmed M. El-Zohry,[†,‡] Omar F. Mohammed,[‡,§] and Majed Chergui*[,†]

[†]Ecole Polytechnique Fédérale de Lausanne, Laboratoire de Spectroscopie Ultrarapide (LSU), ISIC, Faculté des Sciences de Base, station 6, CH-1015 Lausanne-Dorigny, Switzerland

[‡]Chemistry Department, Faculty of Science, Assiut University, Assiut 71516, Egypt

ABSTRACT: Measurements of the ultrafast broadband UV fluorescence of *N*-acetyltryptophanamide (NATA) provide detailed information on its relaxation patterns in three different solvents: methanol (MeOH), water and acetonitrile (ACN). Several processes leading to excited state solvation and cooling are found to occur on different characteristic time scales and are thoroughly analyzed. Comparison between protic MeOH and aprotic ACN allows one to single out a 12 ps component in the former, which is attributed to the rearrangement of H-bonds existing between the protic solvent and excited NATA. This significantly stabilizes the excited state and provides the molecule with an efficient cooling mechanism. The corresponding dynamics in water are much faster (<1.5 ps). Comparison with static spectroscopic properties stresses the role of site-specific H-bonding in controlling the fluorescence quantum yield of NATA in protic solvents. These findings are consistent with existing models that describe tryptophan quenching as a result of charge transfer from the indole to the amide assisted by H-bonding at the carbonyl site.

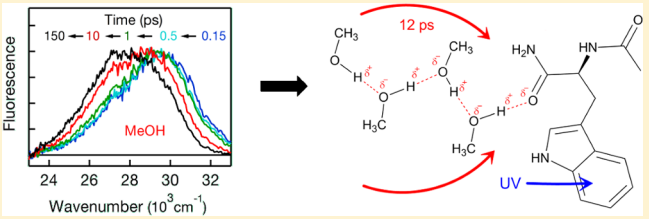

1. INTRODUCTION

The high sensitivity of the indole fluorescence to the environment makes this UV chromophore an efficient optical probe of the changes of the local electrostatic conditions of its surroundings.[1−3] In particular, the peak emission wavelength and quantum yield of the indolic amino acid tryptophan (Trp) widely change from protein to protein, and upon any modification of the protein in the location where it resides. Thus, Trp fluorescence is routinely used to monitor protein changes such as folding/unfolding dynamics, conformational rearrangements and binding of ligands to active enzymatic sites.[4−7] Monitoring Trp fluorescence is even used to noninvasively diagnose malignancy in cells.[8,9] Recently, ultrafast time-resolved UV spectroscopic techniques have come into this picture, further expanding the extent to which indolic optical activity can be used to probe ongoing physicochemical processes. For instance, ultrafast transient absorption measurements of Trp located in an appropriate position are sensitive to charge redistributions and nuclear rearrangements, upon photoexcitation of a cofactor.[10−12] More generally, ultrafast time-resolved measurements of Trp are a powerful spectroscopic tool that allows direct access to the time scale of local conformational changes, fluctuations and hydration dynamics in biological macromolecules.[13,14] These processes are being intensively investigated as it is believed that internal motions occurring on a hierarchy of time scales, all the way down to subpicosecond, play a key role in the biological activity of proteins.[15−17]

N-Acetyltryptophanamide (NATA) is a molecular analogue of tryptophan which can be introduced in model systems such as micelles and used as an optically active probe to study solvation and conformational dynamics.[18] It has the advantage of featuring a single lifetime (3 ns in water at room temperature), unlike tryptophan, which shows two lifetimes attributed to different rotameric structures.[19,20] In addition, the structure of NATA (Figure 1) is considered a more accurate representation of the form by which indole is embedded in a protein.[21] Indeed, it contains two amide groups that resemble peptide bonds constituting the protein backbone, and it does not adopt the zwitterionic form that is dominant for Trp in water at neutral pH because the amino and carboxylic groups are uncharged in NATA due to acetylation of the amine and amide formation of the carboxylic group. Last, the solubility of NATA in water is much greater than that of tryptophan, improving substantially the signal-to-noise ratio in time-resolved experiments.

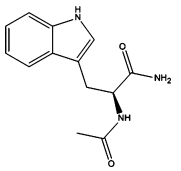

Figure 1. Structure of *N*-acetyltryptophanamide (NATA).

Received: June 1, 2012
Revised: July 27, 2012
Published: August 14, 2012

Spectroscopic applications of indole and its derivatives require a detailed understanding of their fundamental photophysics. For instance, since in ultrafast fluorescence studies of proteins it is often difficult to separate water-related solvation effects from emission shifts directly arising from motions of the protein itself,[22] several works have pursued the full comprehension of the solvation dynamics of isolated Trp or of small peptides in water solution, in order to provide a starting point for the interpretation of the results obtained in more complex systems.[20,23−27] Recent broadband UV fluorescence upconversion measurements of Trp in water, aided by molecular dynamics simulations, provided a detailed characterization of its solvation dynamics featuring three relaxation time scales of <10 fs, ∼0.2 ps, and ∼1 ps.[20] Beyond solvation dynamics, another important issue still debated concerns the mechanism(s) leading to emission quenching of indole residues.[28−31] Indeed, Trp quenching could also act as a biologically relevant protection mechanism of some proteins against photodamage by natural UV light. Based on both static and time-resolved measurements of several proteins, it has been often proposed that Trp fluorescence can be quenched by specific amino acids acting as acceptors of proton or electron-transfer processes from the excited chromophore if sufficiently close to it.[30,32] Recently, two general models have been proposed in the literature,[28,29] according to which the basic photochemical process quenching the emission of Trp embedded in a protein is intramolecular in nature, while nearby residues or water molecules can indirectly modulate its efficiency, yielding the wide variability of Trp quantum yields in proteins.

The first of these models suggested that aromatic systems such as indole can be quenched via a nonradiative transition from the initially excited L_a ($\pi-\pi^*$) state to a predissociative charge-transfer (CT) $\pi-\sigma^*$ state antibonding in the NH stretching coordinate of indole.[28,33] Since the gap between L_a and $\pi-\sigma^*$ states is strongly sensitive to any external electric field,[28] this mechanism could explain the variations of the Trp quantum yield in different proteins, where Trp experiences very different environments. This model, however, was criticized on the grounds that the quantum yield of the light-absorbing portion of Trp, well represented by 3-methylindole, shows only a weak solvent dependence while one would expect interaction with polar solvents to strongly stabilize the CT state and favor quenching.[34,35] The second mechanism involves CT from the excited indole to the lowest unoccupied π^* orbital of a nearby amide moiety.[19,29,35,36] In this scenario the closest amide group belonging to the protein backbone provides a quenching channel available to any intraprotein Trp, and the position of nearby residues or water molecules indirectly influences the emission yield by determining the relative electrostatic potential of the indole ring with respect to the amide. Hybrid quantum mechanical/molecular mechanics (QMMM) molecular dynamics (MD) simulations provided strong evidence that this model allows one to rationalize the wide variety of Trp quantum yields found in proteins.[29,37] In this context, it is worth noting that quenching mechanisms affecting a free Trp in solution are not necessarily representative of actual intraprotein processes.[21] Indeed, the quantum yield of a Trp in H_2O is pH- and conformer-dependent because of the role played by the charged ammonium group.[21,38,39]

An important aspect of indole-to-amide CT concerns the proposed role of H-bonding. Calculations suggested that the dominant stabilization mechanism of the CT state of NATA in water is H-bonding to the carbonyl site of the electron-accepting amide, eventually leading to a decrease of emission quantum yield.[35] Such interplay between H-bonding and CT is a general problem in biology and chemistry.[40−42] For instance, a proton-coupled intramolecular electron transfer process was evidenced in DNA[40] suggesting that such H-bond assisted CT events may play a vital role in some biological reactions. Recent work studied in detail the case of formylperylene (FPe),[41,42] where ultrafast CT from the perylene unit to the formyl group is drastically facilitated by H-bonding between the carbonyl oxygen of FPe and H-donating solvents. Thus, a comparable mechanism could enhance CT from excited indole to a close amide acceptor and quench fluorescence whenever the amide becomes the H-bond acceptor or experiences a comparable short-range interaction.

In order to address the issue of site-specific solvation due to H-bonding and to understand the influence it has on fluorescence quenching by affecting the nature and the energy of the excited electronic states, we carried out static absorption/emission and ultrafast UV fluorescence measurements of NATA in several solvents differing by their polarity and their H-bond capabilities. The results clearly show that H-bonding interactions between protic solvents and NATA play a major role in quenching the fluorescence from the excited molecule. In addition, this study extends our previous work on Trp in water,[20] in that comparing the relaxation dynamics of the indolic emission in different solvents provides valuable information to decipher and decouple different competing processes.

2. EXPERIMENTAL METHODS

The experimental setup used for the ultraviolet (UV) broadband fluorescence upconversion measurements is described in detail in refs 20 and 43, and only its main features are highlighted here. A Coherent-RegA Ti:sapphire regenerative amplifier was operated at 150 kHz and provided 800 nm pulses of 4 μJ typical energy and 80 fs duration. This beam was used to pump an optical parametric amplifier (Coherent, OPA-9400) typically yielding 65 fs pulses (after an external prism compressor) of 300 nJ maximum pulse energy and 15 nm full width at half-maximum (fwhm). Finally, excitation pulses at 290 nm of typically ∼20 nJ were obtained by frequency doubling in a 0.1 mm β-barium borate (BBO) crystal the OPA output at 580 nm. The excitation beam was focused down to a 30 μm spot inside a 0.2 mm thick UV-grade glass flow cell where the sample was continuously circulated at room temperature at a typical speed of 1 m/s in order to avoid photodamage. Emission from the sample was collected by a parabolic mirror in forward-scattering geometry, and directed to a second mirror that focused it to a 0.25 mm thick BBO crystal. The emission was then upconverted by mixing it with a gate pulse at 800 nm obtained from a portion of the fundamental beam. A waveplate was used to control the relative polarization of gate and excitation beams. Finally, the upconverted signal was spatially filtered and detected with a spectrograph and a liquid-N_2-cooled charge-coupled device (CCD) camera. Rotation of the BBO crystal by a computer-controlled motor during the accumulation time of the CCD allowed acquiring the full emission spectrum at each delay between excitation and gate pulses. The instrument response function (IRF) of the setup is 190 fs as measured by the fwhm of a kinetic trace of the Raman line of H_2O. Each measurement reported here was obtained by averaging 10−20 scans.

dx.doi.org/10.1021/jp305363y | J. Phys. Chem. B 2012, 116, 10730−10738

Technical details on how moment analysis is performed on fluorescence upconversion data can be found in ref 20.

Samples consisted of solutions of *N*-acetyl-L-tryptophanamide (NATA) in deionized H_2O, acetonitrile (ACN), methanol (MeOH), dioxane (Dox), deuterium oxide (D_2O), methanol-d_4, and perdeuterated acetonitrile (ACN-d_3). NATA and all the solvents were obtained from Sigma-Aldrich. When performing fluorescence upconversion measurements, the concentration of the molecule in solution was chosen to be ~3 mM in order to have approximately 0.3 OD absorption through the flow cell at the excitation wavelength. Static absorption and emission measurements were carried out on a Shimadzu UV-3600 spectrophotometer and a Shimadzu RF-5301PC spectrofluorometer, respectively. Both static and time-resolved emission measurements were corrected for the spectral response and dispersion of the detecting system.

3. RESULTS

Figure 2 shows the normalized static absorption and emission spectra of NATA in 4 different solvents with widely different

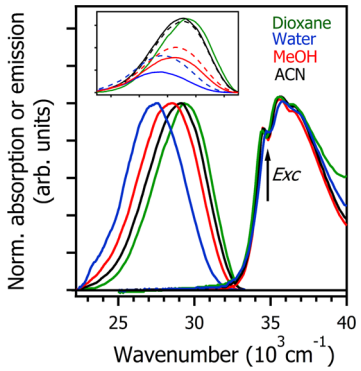

Figure 2. Normalized static absorption and emission spectra (290 nm excitation) of NATA in different solvents. Inset: non-normalized emission spectra of NATA in H_2O, MeOH, ACN (full lines) and in the deuterated solvents D_2O, methanol-d_4, and ACN-d_3 (dashed lines), for samples having the same optical density at the excitation wavelength of 290 nm.

dielectric constants and H-bonding abilities: 1,4-dioxane (ε = 2.3, aprotic), acetonitrile (ACN, ε = 37.5, aprotic), methanol (MeOH, ε = 33, protic), and water (ε = 80, protic). The overall polarity of the solvents can be alternatively estimated on the empirical Dimroth–Reichardt scale E_T^N (Table 1).[44] The samples have the same optical density at the excitation wavelength of 290 nm. Consequently, the emission intensity (see inset) is proportional to the fluorescence quantum yield. The absorption band is only weakly solvent-dependent, while strong variations in intensity and energy are seen in emission. Broadly speaking, the emission shifts to the red and becomes broader with increasing solvent polarity (Table 1). The inset shows a pronounced quenching effect: indeed, by comparing the area of the band in different solvents we get the following relative emission quantum yields (see also Table 1): $\phi_{ACN} = 1.06\phi_0$, $\phi_{MeOH} = 0.52\phi_0$, $\phi_{H2O} = 0.29\phi_0$, where ϕ_0 is the quantum yield of NATA in 1,4-dioxane. Upon deuteration of ACN (see inset) we observe almost no variation of quantum yield ($\phi_{ACN\text{-}d3} = 0.95\phi_{ACN}$), while strong changes are induced by isotopic substitution in both MeOH ($\phi_{methanol\text{-}d4} = 1.29\phi_{MeOH}$) and water ($\phi_{D2O} = 1.84\phi_{H2O}$).

Figure 3 displays the time-energy plot of the fluorescence of NATA in water detected at magic angle after optical excitation

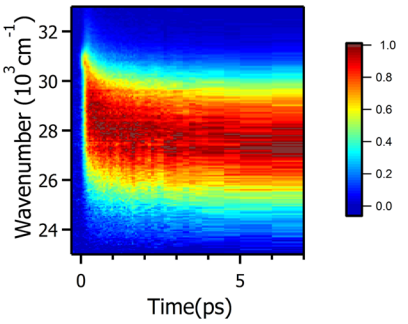

Figure 3. Time–wavenumber plot of the fluorescence spectrum of NATA in water, measured by fluorescence upconversion upon excitation with 290 nm pulses of 20 nJ energy. Intensity is color-coded according to the legend on the right side of the graph.

at 290 nm. There is a clear dynamical Stokes shift due to the gradual solvation of the excited molecule, which occurs within the first picosecond without important intensity variations. Figure 4 shows the normalized emission spectra at

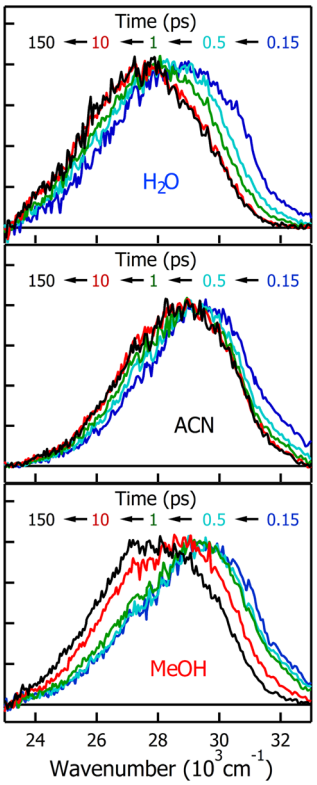

Figure 4. Normalized emission spectra of NATA in water, ACN, MeOH detected at different delays after excitation at 290 nm.

representative time delays. It can be clearly seen that the dynamical shift is complete in a few picoseconds and is accompanied by a small narrowing of the band. Similar measurements in ACN and MeOH are also shown in Figure 4. The most reliable way to compare the relaxation dynamics of NATA in the three solvents is to carry out a moment analysis of the time-resolved emission band. The zeroth moment (i.e., the area of the emission band, not shown) does not exhibit any

dx.doi.org/10.1021/jp305363y | J. Phys. Chem. B 2012, 116, 10730–10738

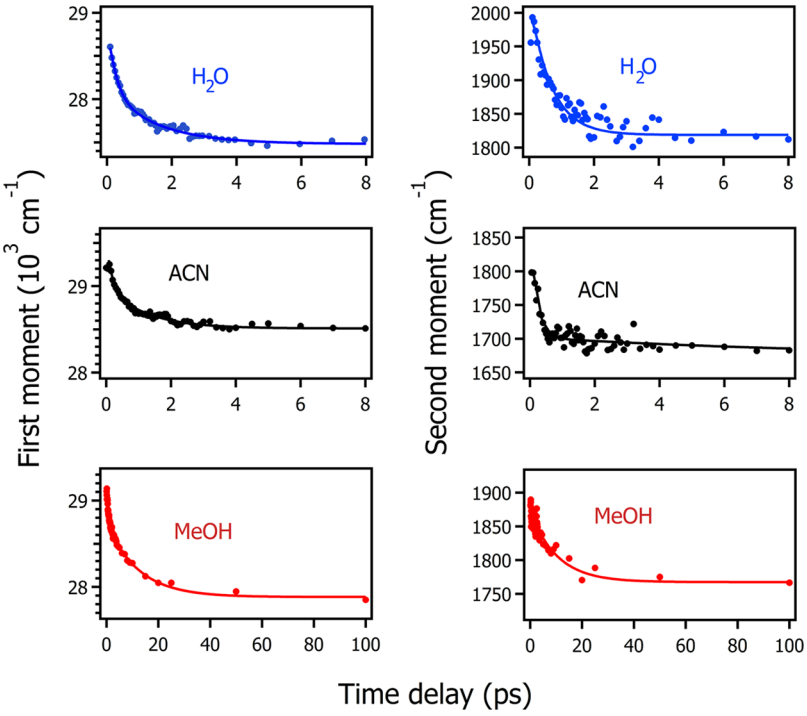

Figure 5. First (left panels) and second (right panels) moment of the emission band of NATA in three solvents at different delay times upon 290 nm excitation. The continuous curves are fits with an appropriate function describing a multiexponential evolution, convoluted with the instrumental response function.

Table 1. Dielectric Constant (ε_0), Dimroth−Reichardt Polarity Parameter (E_T^N),[44] Steady-State Absorption (ν_{max}^{abs}) and Fluorescence (ν_{max}^{em}) Maxima, and Fluorescence Quantum Yields (ϕ_{rel}) of NATA Relative to That in 1-4-Dioxane in the Various Solvents; Decay Times and Amplitudes Obtained by Single or Biexponential Fits of the First and Second Moments Reported in Figure 5[a]

solvent	1,4-Dox	ACN	ACN-d_3	MeOH	methanol-d_4	H_2O	D_2O
ε_0	2.3	37.5	37.5	33.0	32.7	80.0	78.5
E_T^N	0.16	0.46		0.76		1.00	
ν_{max}^{abs} (cm^{-1})	35600 ± 100	35600 ± 100		35600 ± 100		35800 ± 100	
ν_{max}^{em} (cm^{-1})	29400 ± 100	29100 ± 100	29100 ± 100	28500 ± 100	28600 ± 100	27200 ± 100	27500 ± 100
ϕ_{rel}	ϕ_0	1.06ϕ_0	1.00ϕ_0	0.52ϕ_0	0.67ϕ_0	0.29ϕ_0	0.53ϕ_0
			First Moment				
τ_{11} (ps)		0.10 ± 0.03		0.74 ± 0.14		0.24 ± 0.08	
S_1 (cm^{-1})		800 ± 200		410 ± 40		840 ± 120	
τ_{12} (ps)		1.2 ± 0.2		12.1 ± 1.4		1.5 ± 0.2	
S_2 (cm^{-1})		490 ± 40		890 ± 40		640 ± 100	
			Second Moment				
τ_{21} (ps)		0.18 ± 0.06		10 ± 2		0.7 ± 0.2	
N_1 (cm^{-1})		180 ± 40		110 ± 10		190 ± 20	
τ_{22} (ps)		10 (fixed)					
N_2 (cm^{-1})		30 ± 10					

[a]The corresponding best-fit curves are shown in Figure 5. 1,4-Dox = 1,4-dioxane, ACN = acetonitrile, ACN-d_3 = trideuteroacetonitrile, MeOH = methanol, methanol-d_4 = tetradeuteromethanol. The uncertainties on the time constants and shifts obtained by moment analysis are the statistical errors (95% confidence) obtained by the fitting procedure. The uncertainties on the peak positions of the static spectra represent instrumental errors.

appreciable variation in the first 200 ps. This is not surprising since the room temperature lifetime of the molecule is in the nanosecond range. The time dependence of the first (center of mass of the emission energy) and second (width of the emission band) moments in all three solvents are reported in Figure 5 and exhibit a clear solvent dependence.

The dynamics in ACN consists of a total shift of about 700 cm^{-1} within the first few picoseconds, accompanied by a narrowing which, to a large extent, occurs on a comparable time scale. As expected from Figure 2, in MeOH the total Stokes shift is significantly larger. Time-resolved data, on the other hand, show that part of this shift occurs on a long (>10 ps) time scale where changes are no longer observed in ACN (see also Figure 4). A band narrowing (130 cm^{-1}) also takes place in MeOH, again on a much slower time scale (several picoseconds) than in ACN. Finally, in water both the shift and the narrowing are largest, and the whole dynamics occurs within the first few picoseconds. Fitting these data with appropriate

dx.doi.org/10.1021/jp305363y | J. Phys. Chem. B 2012, 116, 10730−10738

functions representing first- and second-moment dynamics convoluted with our IRF[20] allows to one quantify these behaviors (see Table 1): the evolution of the first moment turns out to be biexponential in all three solvents, with the following components: In ACN, we find spectral shifts of 800 ± 200 cm^{-1} and 490 ± 40 cm^{-1} with characteristic time constants of 0.10 ± 0.03 ps and 1.2 ± 0.2 ps respectively, for MeOH spectral shifts of 410 ± 40 cm^{-1} and 890 ± 40 cm^{-1} with time constants of 0.74 ± 0.14 ps and 12.1 ± 1.4 ps, respectively, and for water 840 ± 120 cm^{-1} and 640 ± 100 cm^{-1} with 0.24 ± 0.08 ps and 1.5 ± 0.2 ps, respectively. The kinetics of the second moment can be reproduced by a single exponential in water, a 190 ± 20 cm^{-1} narrowing taking place in 0.7 ± 0.2 ps, and in MeOH, where the narrowing is 110 ± 10 cm^{-1} in 10 ± 2 ps. The corresponding values in ACN are 180 ± 40 cm^{-1} and 0.18 ± 0.06 ps, respectively, but in this case an additional small (30 ± 10 cm^{-1}) slower narrowing (whose time constant was fixed to 10 ps) must be introduced to fully reproduce the data at the longest times.

4. DISCUSSION

4.1. Static Properties. Figure 2 and Table 1 show that the fluorescence undergoes much larger solvatochromic shifts than the absorption. Assuming a purely dielectric solvation, this would indicate a strong increase of the permanent dipole moment of NATA upon photoexcitation,[1] which is consistent with the well-studied electronic properties of indole, featuring a ground state dipole moment of 2 D and dipole moments of 2−3 D and 6−8 D in its excited L_b and L_a states, respectively.[28,45,46] However, the same data also provide a clear signature of the substantial role of site-specific H-bonding interactions between the molecule and protic solvents. In fact, it turns out that the main parameter controlling emission quenching, while also contributing to the emission shift, is the H-bonding ability of the solvents rather than their dielectric properties.[47] Indeed, only a small emission peak shift and basically no intensity variation (within experimental uncertainty) is observed when going from a weakly polar solvent like dioxane to a polar aprotic ACN, despite the significant increase of both the dielectric constant and the polarity parameter E_T^N (see Table 1). Thus, the quantum yield is not significantly altered when the molecule is solvated by a purely dielectric mechanism. In sharp contrast to this, a large spectral shift and an obvious quenching is observed from aprotic ACN to protic MeOH. Since these two solvents have very close dielectric constants and similar molecular structures, but differ in their H-bonding ability, one can assume that the difference between them is the effect of H-bonding. The supplementary H-bonding ability of MeOH is actually reflected in its higher polarity E_T^N as compared to ACN. Finally, both quenching and red spectral shift are further enhanced when going to H_2O, which is a stronger H-bond donor than MeOH. These results fully confirm those by Callis et al.,[35] who reported emission quantum yield of NATA in a wide range of solvents, including alcohol chains of different lengths, providing clear evidence of a correlation between quantum yield and H-bonding ability of the solvent. Furthermore, the effects upon deuteration of the solvents provide conclusive evidence in the same direction, because almost no difference is observed in either shape or quantum yield upon deuteration of ACN, while a variation of the emission peak position and a strong change of the emission quantum yield is induced by isotopic substitution in both MeOH and Water. Previous static measurements on 3-methylindole, which can be taken as the "pure" light-absorbing portion of the molecule, showed no significant dependence of the quantum yield ϕ on H-bonding. It was found that ϕ = 0.34 in a wide range of solvents, very close to the value of NATA in dioxane (0.36).[35,38] The overall set of results implies that an additional quenching channel is activated when a H-bonding interaction is established between a solvent and NATA. At the same time, the difference between NATA and 3-methylindole suggests that the molecular site where the bond is established is not located on the indole moiety. This tentatively suggests the two carbonyl oxygen atoms in NATA as the most likely sites accepting an H-bond, leading to a Stokes shift and somehow causing the emission quenching observed in Figure 2. Although a conclusive identification of the acceptor site would require a structurally sensitive approach such as IR spectroscopy, this interpretation is consistent with the previously proposed model of emission quenching by charge transfer from indole to amide,[19,36] and with recent results obtained by mixed QM/MM simulations indicating that the empty π^* orbital on the amide accepting the electron can be stabilized by H-bonding at the C═O site, thus supporting this quenching channel.[35] The occurrence of these site-specific interactions is further supported by temporally resolving the solvation dynamics of NATA, which provide evidence of the buildup of the H-bond between the molecule and the protic solvent after excitation.

4.2. Solvation Dynamics of NATA in MeOH and ACN: Role of H-Bonding. We first compare the fluorescence upconversion results in ACN and MeOH. The first moment kinetics in MeOH (Figure 5 and Table 1) clearly shows a 12 ps component, which is responsible for the major part (890 cm^{-1}) of the relaxation and is totally absent in ACN where all dynamical events are over in <3 ps. On the other hand, in MeOH an additional 410 cm^{-1} Stokes shift occurs in 0.7 ps, quite close in magnitude to one of the two components observed in ACN where the emission peak shifts by 490 cm^{-1} in 1.2 ps. These data can be interpreted by attributing the 0.7 ps (1.2 ps) in MeOH (ACN) to non-site-specific polar solvation, which is expected to cause similar Stokes shifts in the two solvents due to their very similar dielectric constants. Conversely, the long (12 ps) component in MeOH which is completely absent in ACN can be attributed to H-bond dynamics between the solvent and NATA, which accounts for most of the energy relaxation when the molecule is in the protic solvent.

A similar component of 15 ps was found for the solvation dynamics in MeOH of coumarin 153, capable of accepting a H-bond at its C═O group.[48] Recent studies of the ultrafast relaxation of formylperylene in MeOH[41,42] found a 13.4 ps dynamics, which was attributed to an H-bond interaction between the solvent and the carbonyl oxygen of the molecule. This conclusion was based on experiments in binary mixtures of MeOH and ACN, and on the absence of such dynamics in nitroperylene,[49] where the C═O moiety is substituted by a nitro group and such site-specific interactions are supposedly weakened. In the case of a molecule already forming a strong H-bond in the ground electronic state, a few experiments have been able to observe in real time the local rearrangement or cleavage of the bond in response to photoexcitation of the probe.[50−53] For instance, femtosecond IR spectroscopy was used to track the local changes of the H-bond linking coumarin 102 to a hydrogen donating molecule.[51−54] These measurements provided a clear-cut signature of the H-bonding dynamics by time-resolving large spectral shifts of some

characteristic vibrational marker modes which are involved in hydrogen bond formation. The overall result of these works is that local H-bond rearrangement and/or cleavage is ultrafast (100−250 fs).[50−54] Such a fast response can be understood based on the fact that this phototriggered reorganization actually only requires the relative motion of two strongly interacting atoms. On the other hand, 2D-IR spectroscopy was recently used[55,56] to investigate H-bonding between MeOH and the C═O site of *N*-methylacetamide, which coexists in two comparable populations of bonded and nonbonded molecules at equilibrium. It was found that formation and breaking of the H-bond between the molecule and the solvent takes place on typical time scales of 10−15 ps, an average H-bond lifetime of 12 ps being estimated by molecular dynamics simulations. On the whole, comparison with these results supports our attribution of the 12 ps component in Table 1 to H-bond network dynamics. Recent work has convincingly proven that the H-bonding dynamics cannot be pictured as arising from a simple bimolecular interaction, because the acceptor site on the molecule becomes the terminal point of a network of several MeOH molecules linked via H-bonds.[41] This model was put forward to explain the 13.4 ps solvation dynamics of formylperylene in MeOH mentioned above: experiments in binary mixtures where MeOH molecules are dispersed in aprotic ACN allowed a continuous change of the fraction of ground-state molecules bonded to MeOH, and proved that the >10 ps hydrogen bonding dynamics actually represents a collective rearrangement of the entire H-bonding network after photoexcitation of the probe.[41] All molecules are expected to equally contribute to this >10 ps relaxation, independent of whether they already formed an H-bond with the solvent in the ground state. The agreement with the time scale found here leads to the conclusion that this kind of collective H-bonding network formation also occurs around the acceptor site of excited NATA.

Before proceeding to compare these results with those in water, we complete the discussion of NATA in ACN and MeOH by addressing the other solvation time scales found by the analysis of the first moment. First, both solvents show polar solvation on a time scale of the order of 1 ps (0.74 ps in MeOH, 1.2 ps in ACN), which is fairly consistent with previous literature. Several studies on the solvation dynamics in ACN exhibited a component between 0.6 and 1.3 ps,[42,48,57] consistent with our results and ultimately ascribable to collective reorganization of the solvent via rotational and translational motions. For MeOH, the 0.74 ps time scale we find for dielectric solvation is also comparable to previous findings (1.6 ps,[42] 1.0 ps,[57] biexponential with 0.3 and 3 ps components of comparable weight[48]). While on the whole these numbers convincingly fix around 1 ps the time scale on which polar solvation occurs for both solvents, the appreciable dispersion of the values probably reflects some degree of dependence of the process on the choice of the probe solute, or even on the way the data are analyzed. Finally, the data for ACN show an additional fast (0.1 ps, 800 cm^{-1}, see Table 1) dynamics which appears to have no equivalent in the other two solvents. This process must be interpreted as evidence for inertial solvation,[58,59] which is normally regarded as the fastest contribution to the dynamic Stokes shift. In ACN, computational and experimental studies found that inertial solvation occurs on a time scale between 70 and 120 fs and normally accounts for the major portion (up to 80%) of the total relaxation.[48,57−61] The value of about 60% in 0.1 ps we find here (see Table 1) is consistent with this view. Since the inertial dynamics is expected to be Gaussian (as opposed to exponential),[58] we also tried to fit the first moment kinetics observed in ACN by the sum of a Gaussian (of 0.1 ps effective decay time scale) and an exponential decay, both convoluted with our Gaussian IRF. The resulting fit is as good as the biexponential one, the only difference being a reduction to 1.0 ps of the longer decay time associated with polar solvation. This only means that our IRF is not short enough to discriminate between these two functional forms and does not affect our interpretation. On the other hand, the time scale of inertial solvation in MeOH is believed to be significantly faster (30−50 fs) than in ACN,[48,62,63] and thus well below our ability to resolve it, and it is comparatively smaller, typically contributing to 10−30% of the total Stokes shift. This is consistent with our finding that the values of the first moment in ACN and MeOH are close to each other at time zero (Figure 5), because actually the time-zero value we measure in MeOH should already be deprived of its (unobservable) inertial component.

4.3. Solvation Dynamics in Water. Inertial solvation in water is generally considered to occur in well below 0.1 ps and to account for at least half of the total relaxation energy.[58] Recent MD simulations on tryptophan concluded to a value as low as 10 fs,[20] clearly unobservable within our resolution, the only indirect effect being the significantly lower value of the time-zero first moment we observe for NATA in water (Figure 5). As for the other 0.24 and 1.5 ps components, their time scales are fairly consistent with previous studies of Trp and other systems.[20,23] Based on our conclusions in the previous paragraph, it is tempting to attribute the 1.5 ps component in water to H-bonding and the 0.24 ps component to solvation via a dipolar mechanism. However, contrary to MeOH where the 0.74 and 12 ps components are well separated, in the case of water it is probably an oversimplification to relate the 1.5 ps component exclusively to H-bonding. Another reason for this is that the amplitude of the associated shift is slightly smaller in water (640 cm^{-1}) than in MeOH (890 cm^{-1}), whereas water is a stronger H-bond donor than MeOH. Thus, it is probably safer to assign the 1.5 ps component as an upper limit for the H-bonding time scale between NATA and water. This being said, the almost 10 times faster H-bonding dynamics in water than in MeOH is indeed supported by the existing literature, as explained below.

Continuous dielectric models of solvation relate the fast solvation response of water to some of its macroscopic dielectric properties, particularly its subpicosecond Debye relaxation times and its very high polarity.[64,65] However, these models give no direct information on the molecular details of solvation, which are central in site-specific interactions such as H-bonding. Indeed, the dynamics of hydrogen bonds and H-bonding solvation at molecular acceptor sites like C═O are still less understood and subject to intense investigation.[66−71] For instance, recent studies[66−69] of the internal H-bond dynamics in liquids by ultrafast IR spectroscopy attempted to assess the time scale on which an initially nonequilibrium distribution of H-bonds evolves toward a new thermal equilibrium. For water, it was concluded that the typical time scale of H-bond network rearrangement is on the order of 1 ps (values between 0.5 and 2 ps were reported), consistent with the present results. It is worth mentioning that longer times of 3−4 ps were recently reported for the formation of a hydrophobic solvation shell around halogen solutes.[72] As for alcohols, several studies addressed the relaxation of their

intrinsic H-bond network,[68,69] or the dynamics of H-bonding between the alcohol and a probe molecule in the excited electronic state.[70,71] These data suggest a more complex dynamics than water. Two studies[68,69] found that the H-bond network dynamics in MeOH relax on multiple time scales, including components between 7 and 20 ps. The striking difference between water and alcohols was attributed partly to the lower mass of water molecules, and partly to the fact that only H_2O is able to form a truly three-dimensional H-bonded network that allows a very efficient redistribution of energy. Thus, these results also make it reasonable to identify the 12 ps component in MeOH, and tentatively the 1.5 ps component in water, as typical time scales for the rearrangement of H-bonds between the solvents and NATA. Photoinduced H-bond strengthening can be explained if the excitation instantaneously increases the charge density on the molecular site accepting the hydrogen bond. As argued before, this is most likely the carbonyl site. The augmented charge on the acceptor site will attract protons and trigger the formation of a novel H-bond or the strengthening of the existing interaction via collective H-bond network formation. The 12 ps dynamics we observe in MeOH is a real-time observation of this process that in water occurs (at most) in 1.5 ps.

4.4. The Cooling Dynamics. A common cause of emission band narrowing over a 1−10 ps time scale is cooling,[57,65,73] which is sometimes observed to have its own characteristic time scales, not necessarily solvation-driven.[43,73] While this seems to be the case for the very small (30 cm^{-1}) and longest (10 ps) narrowing component observed in ACN, all the other time scales of the second moment detected for NATA are actually comparable to first moment ones, and thus, they need to be discussed in relation to solvation. General evidence coming from data in Figure 5 is the striking solvent-dependence of the time scale over which the emission band narrows down. This indicates that microscopic details of the solute−solvent interaction play a major role in controlling the cooling dynamics.

In MeOH, the narrowing of about 10 ps is in good agreement with the 12 ps H-bonding formation time. This strongly suggests that H-bonding to the solvent provides an efficient channel to dissipate the excess thermal energy to the solvent, especially considering that no cooling is observed in the same solvent on the time scale (0.74 ps) of polar solvation. One may understand this because polar solvation mainly arises from dipolar interactions in which internal vibrational degrees of freedom of the solute are not involved, whereas H-bonding introduces a strong local link to the solvent network allowing vibrational energy to be dissipated along the binding coordinate.

In H_2O the interpretation is less straightforward, because cooling occurs on an intermediate time scale (0.7 ps) between the two times (0.24 and 1.5 ps) found from the Stokes shift. Again, we believe this to arise from the fact that one cannot fully identify the 1.5 ps component with H-bonding in water, but also in this case H-bonding most likely provides the major channel through which excess vibrational energy is dissipated.

In ACN the emission band evolves in less than 0.2 ps, much closer to the inertial solvation time scale (0.1 ps) than to that (1.2 ps) of polar solvation, so that it is natural to associate this narrowing to ongoing inertial solvation. On the one hand this readily explains why the total narrowing resolved in ACN is larger than in the other two solvents (see Table 1 and Figure 5), since the equivalent dynamics in H_2O and MeOH are not observable within our IRF. On the other hand, although its <0.2 ps time scale is shorter than usual cooling times, we propose this dynamics to represent an ultrafast cooling process mainly driven by the same solvent rearrangements that cause inertial solvation. Indeed, since the latter involves close-range interactions with proximal solvent molecules, it is expected to allow dissipation of excess vibrational energy much more efficiently than polar solvation does, leading to the possibility of an ultrafast "local" cooling. For comparison, ultrafast fluorescence measurements of the protonated Schiff base of retinal in ACN found the emission band to appear cold (i.e., with a mirror-image profile with respect to the absorption band) on very short time scales after photoexcitation, suggesting ultrafast cooling effects to be operative.[74,75] Very fast (0.2−0.3 ps) cooling dynamics have recently been evidenced for UV dyes in several solvents.[73] Also the expectation of comparable total cooling in all three solvents supports the same interpretation, because the additional 7 ps dynamics measured in ACN is too small (30 cm^{-1}) to account for the overall narrowing we expect, based on our findings in MeOH and water. Finally, we can reasonably rule out internal vibrational redistribution (IVR) to be at the origin of this dynamics, because it would be solvent-independent, and typical time scales of IVR are estimated to be much faster (~10 fs).[76]

4.5. The Quenching Mechanism. The additional Stokes shift and the decrease of fluorescence quantum yield observed in NATA upon site-specific solvation in protic media imply that it forms much stronger H-bonds upon excitation, and that such interactions eventually favor the nonradiative events leading to quenching. The role of excited state protonation is reflected also in the changes of the emission quantum yield of the molecule in deuterium-substituted solvents. Also time-resolved data prove that photoexcitation triggers the buildup of H-bonds providing significant stabilization of the electronic energy. Finally, comparison with existing data on 3-methylindole[35,38] suggests the carbonyl site of NATA as the acceptor site of the H-bond.

Since the excited state lifetime of NATA is much longer (ns) than typical solvation times (Table 1), the dynamics observed here do not represent the nonradiative transition in itself, because quenching actually occurs with a slow (ns^{-1}) rate from the fully solvated excited state. Thus, quenching will be ultimately driven by solvent fluctuations around the equilibrium configuration reached after completion of the dynamics in Figure 5. Stokes shift dynamics (Table 1) actually provides full information on the time scale(s) of fluctuations because (in the limit of linear response) the Stokes shift response function measured by transient fluorescence equals the time correlation function of the equilibrium fluctuations of the transition frequency.[59] As a consequence, the H-bond solvation lifetimes found by our analysis can equivalently be interpreted as average lifetimes of H-bonds continuously forming and breaking between the solvent and the molecule in the equilibrated excited state. Thus, this characteristic time scale must be the main parameter ultimately controlling the emission quantum yield of this system. This view can also explain the increase of quantum yield observed (Figure 2) upon deuteration. In fact, solvation is found to be systematically slower in deuterated solvents.[77−80] In the case of protic solvents like water, this is at least partly due to slower H-bond making and breaking processes in D_2O with respect to H_2O.[77,80] In particular, it is worth noting that going from MeOH to MeOD showed a 10−

50% increase of the ~10 ps solvation scale depending on the probe molecule used.[77,78]

While the above considerations are independent of the specific nature of the quenching transition, our results are fully consistent with the model of emission quenching in NATA or Trp via nonadiabatic CT from the L_a state of indole to the π^* orbital of the amide.[19,35−37] In fact, it was shown that the probability of such an event is enhanced by H-bonding localized on it, stabilizing the π^* orbital on the amide and thus assisting CT and quenching.[29,35,37] Also MD simulations[35] indicated the nonradiative decay rate of NATA to be controlled by the fluctuations of the energy gap between the excited L_a state and the CT state. Faster formation and breaking of H-bonds implies faster fluctuations of the energy gap and thus a larger probability per unit time that the molecule experiences a solvent configuration where crossing of the L_a and the CT states quenches the emission. Since the peptide bond in proteins is chemically equivalent to amide, for Trp fully buried inside proteins, the peptide bond closest to the indole ring is expected to play the role of electron acceptor and provide a natural mechanism for quenching. In this case, rather than by H-bonding, this quenching process might be modulated by the close-by residues promoting or hampering CT to the closest peptide bond through the electrostatic potential they exert on the C═O site with respect to the indole ring.

5. CONCLUSIONS

A comparative study of the solvation dynamics of NATA (*N*-acetyltryptophanamide) in aprotic ACN and protic MeOH, featuring very close dielectric constants, allowed us to single out a site-specific interaction process attributed to the donation of an H-bond from the solvent to the molecule, supposedly on its C═O site. In MeOH, such dynamics occur with a 12 ps time constant, and strongly stabilize the excited state providing the molecule with an efficient dissipation channel of excess vibrational energy. In contrast, no efficient cooling is observed on the time scale of non-site-specific solvation due to dipolar solute−solvent interactions. Measurements in H_2O allow us to conclude that the corresponding time scale of H-bonding dynamics is almost 1 order of magnitude faster than in MeOH. The role of H-bonding was also confirmed by static optical measurements of NATA in ACN, MeOH, H_2O and in their deuterated forms. Formation of a strong H-bond in the excited state is supposedly triggered by an increase of the electronic density on the molecular acceptor site upon photoexcitation. This causes a collective reorganization of the H-bonding network linked to the molecule, which is ultimately responsible for excited-state relaxation. For all three solvents we also estimated time scales of polar solvation, and in ACN we additionally resolve a pulse-limited Stokes shift, which we attribute to inertial solvation. The latter is accompanied by band narrowing indicating efficient ultrafast cooling. Combining time-resolved fluorescence data with static measurements clearly points out the role of H-bonding in promoting emission quenching. Our experimental observations support the existing model of indole emission quenching via charge transfer to amide,[19,35,36] and provide experimental evidence of the role of H-bonding in assisting this process.

AUTHOR INFORMATION

Corresponding Author

*E-mail: Majed.Chergui@epfl.ch.

Present Address

[§]Physical Biology Center for Ultrafast Science and Technology, Arthur Amos Noyes Laboratory of Chemical Physics, California Institute of Technology, Pasadena, CA 91125, USA.

Notes

The authors declare no competing financial interest.

REFERENCES

(1) Lakowicz, J. R. *Principles of Fluorescence Spectroscopy*; Kluwer Academic/Plenum Publishers: New York, 1999.
(2) Callis, P. R. In *Methods Enzymology*; Brand, L., Johnson, M. L., Eds.; Academic Press: 1997; Vol. *278*, pp 113−150.
(3) Pan, C.-P.; Muiño, P. L.; Barkley, M. D.; Callis, P. R. *J. Phys. Chem. B* **2011**, *115*, 3245−3253.
(4) Ervin, J.; Sabelko, J.; Gruebele, M. *J. Photochem. Photobiol. B.: Biol.* **2000**, *54*, 1−15.
(5) Deprez, E.; Tauc, P.; Hervé, L.; Mouscadet, J.-F.; Auclair, C.; Hawkins, M. E.; Brochon, J.-C. *Proc. Natl. Acad. Sci. U.S.A.* **2001**, *98*, 10090−10095.
(6) Sanghera, N.; Pinheiro, T. J. T. *J. Mol. Biol.* **2002**, *315*, 1241−1256.
(7) Gabellieri, E.; Bucciantini, M.; Stefani, M.; Cioni, P. *Biophys. Chem.* **2011**, *159*, 287−293.
(8) Grossman, N.; Ilovitz, E.; Chaims, O.; Salman, A.; Jagannathan, R.; Mark, S.; Cohen, B.; Gopas, J.; Mordechai, S. *J. Biochem. Biophys. Methods* **2001**, *50*, 53−63.
(9) Palmer, G. M.; Kelly, P. J.; Breslin, T. M.; Ramanujam, N. *Photochem. Photobiol.* **2003**, *78*, 462−469.
(10) Schenkl, S.; van Mourik, F.; van der Zwan, G.; Haacke, S.; Chergui, M. *Science* **2005**, *309*, 917−920.
(11) Schenkl, S.; van Mourik, F.; Friedman, N.; Sheves, M.; Schlesinger, R.; Haacke, S.; Chergui, M. *Proc. Natl. Acad. Sci. U.S.A.* **2006**, *11*, 4101−4106.
(12) Léonard, J.; Portuondo-Campa, E.; Cannizzo, A.; van Mourik, F.; van der Zwan, G.; Tittor, J.; Haacke, S.; Chergui, M. *Proc. Natl. Acad. Sci. U.S.A.* **2009**, *19*, 7718−7723.
(13) Qiu, W.; Zhang, L.; Okobiah, O.; Yang, Y.; Wang, L.; Zhong, D.; Zewail, A. H. *J. Phys. Chem. B* **2006**, *110*, 10540−10549.
(14) Chang, C.-W.; Guo, L.; Kao, Y.-T.; Li, J.; Tan, C.; Li, T.; Saxena, C.; Liu, Z.; Wang, L.; Sancar, A.; Zhong, D. *Proc. Natl. Acad. Sci. U.S.A.* **2010**, *107*, 2914−2919.
(15) Benkovic, S. J.; Hammes-Schiffer, S. *Science* **2003**, *301*, 1196−1202.
(16) Argawal, P. K. *J. Am. Chem. Soc.* **2005**, *127*, 15248−15256.
(17) Eisenmesser, E. Z.; Millet, O.; Labeikovsky, W.; Korzhnev, D. M.; Wolf-Watz, M.; Bosco, D. A.; Skalicky, J. J.; Kay, L. E.; Kern, D. *Nature* **2005**, *438*, 117−121.
(18) Pal, S. K.; Peon, J.; Zewail, A. H. *Proc. Natl. Acad. Sci. U.S.A.* **2002**, *99*, 1763−1768.
(19) Petrich, J. W.; Chang, M. C.; McDonald, D. B.; Fleming, G. R. *J. Am. Chem. Soc.* **1983**, *105*, 3824−3832.
(20) Bräm, O.; Oskouei Adjarzadeh, A.; Tortschanoff, A.; van Mourik, F.; Madrid, M.; Echave, J.; Cannizzo, A.; Chergui, M. *J. Phys. Chem. A* **2010**, *114*, 9034−9042.
(21) Lakowicz, J. R. *Photochem. Photobiol.* **2000**, *72*, 421−437.
(22) Nilsson, L.; Halle, B. *Proc. Natl. Acad. Sci. U.S.A.* **2005**, *102*, 13867−13872.
(23) Shen, X.; Knutson, J. R. *J. Phys. Chem. B* **2001**, *105*, 6260−6265.
(24) Zhong, D.; Pal, S. K.; Zhang, D.; Chan, S. I.; Zewail, A. H. *Proc. Natl. Acad. Sci. U.S.A.* **2002**, *99*, 13−18.
(25) Pal, S. K.; Peon, J.; Bagchi, B.; Zewail, A. H. *J. Phys. Chem. B* **2002**, *106*, 12376−12395.
(26) Lu, W.; Kim, J.; Qiu, W.; Zhong, D. *Chem. Phys. Lett.* **2004**, *388*, 120−126.
(27) Xu, J.; Knutson, J. R. *J. Phys. Chem. B* **2009**, *113*, 12084−12089.
(28) Dedonder-Lardeux, C.; Jouvet, C.; Perun, S.; Sobolewsky, A. L. *Phys. Chem. Chem. Phys.* **2003**, *5*, 5118−5126.
(29) Callis, P. R.; Liu, T. *J. Phys. Chem. B* **2004**, *108*, 4248−4259.

(30) Qiu, W.; Li, T.; Zhang, L.; Yang, Y.; Kao, Y.-T.; Wang, L.; Zhong, D. *Chem. Phys.* **2008**, *350*, 154−164.
(31) Xu, J.; Chen, J.; Toptygin, D.; Tcherkasskaya, O.; Callis, P.; King, J.; Brand, L.; Knutson, J. R. *J. Am. Chem. Soc.* **2009**, *131*, 16751−16757.
(32) Chen, Y.; Barkley, M. D. *Biochemistry* **1998**, *37*, 9976−9982.
(33) Sobolewsky, A. L.; Domcke, W.; Dedonder-Lardeux, C.; Jouvet, C. *Phys. Chem. Chem. Phys.* **2002**, *4*, 1093−1100.
(34) Meech, S. R.; Phillips, D.; Lee, A. G. *Chem. Phys.* **1983**, *80*, 317−328.
(35) Muiño, P. L.; Callis, P. R. *J. Phys. Chem. B* **2009**, *113*, 2572−2577.
(36) Chen, Y.; Liu, B.; Yu, H.-T.; Barkley, M. D. *J. Am. Chem. Soc.* **1996**, *118*, 9271−9278.
(37) Callis, P. R.; Petrenko, A.; Muiño, P. L.; Tusell, J. R. *J. Phys. Chem. B* **2007**, *111*, 10335−10339.
(38) Eftink, M. R.; Jia, Y.; Hu, D.; Ghiron, C. A. *J. Phys. Chem.* **1995**, *99*, 5713−5723.
(39) Yu, H.-T.; Colucci, W. J.; McLaughlin, M. L.; Barkley, M. D. *J. Am. Chem. Soc.* **1992**, *114*, 8449−8454.
(40) Trifonov, A.; Buchvarov, I.; Wagenknecht, H.-A.; Fiebig, T. *Chem. Phys. Lett.* **2005**, *409*, 277−280.
(41) Mohammed, O. F.; Kwon, O.-H.; Othon, C. M.; Zewail, A. H. *Angew. Chem., Int. Ed.* **2009**, *121*, 6369−6374.
(42) Mohammed, O. F. *J. Phys. Chem. A* **2010**, *114*, 11576−11582.
(43) Cannizzo, A.; Bräm, O.; Zgrablic, G.; Tortschanoff, A.; Ajdarzadeh Oskuei, A.; van Mourik, F.; Chergui, M. *Opt. Lett.* **2007**, *32*, 3555−3557.
(44) Reichardt, C. *Chem. Rev.* **1994**, *94*, 2319−2358.
(45) Lami, H.; Glasser, N. *J. Chem. Phys.* **1986**, *84*, 597−604.
(46) Callis, P. R. *J. Chem. Phys.* **1991**, *95*, 4230−4240.
(47) It is worth noting that the substantial role of H-bonds on solvatochromic properties of NATA, together with the small number of aprotic solvents used in this study, makes it impossible to extract from the data a reliable estimate of ground state and excited state dipole moments of the molecule. Nevertheless, such values are not needed for successive analysis since the main focus of this work is on the effects induced by H-bonding.
(48) Horng, M. L.; Gardecki, J. A.; Papazyan, A.; Maroncelli, M. *J. Phys. Chem.* **1995**, *99*, 17311−17337.
(49) Mohammed, O. F.; Vauthey, E. *J. Phys. Chem. A* **2008**, *112*, 3823−3830.
(50) Pines, E.; Pines, D.; Ma, Y.-Z.; Fleming, G. R. *ChemPhysChem* **2004**, *5*, 1315−1327.
(51) Chudoba, C.; Nibbering, E. T. J.; Elsaesser, T. *Phys. Rev. Lett.* **1998**, *81*, 3010−3013.
(52) Chudoba, C.; Nibbering, E. T. J.; Elsaesser, T. *J. Phys. Chem. A* **1999**, *103*, 5625−5628.
(53) Nibbering, E. T. J.; Tschirschwitz, F.; Chudoba, C.; Elsaesser, T. *J. Phys. Chem. A* **2000**, *104*, 4236−4246.
(54) Palit, D. K.; Zhang, T.; Kumazaki, S.; Yoshihara, K. *J. Phys. Chem. A* **2003**, *107*, 10798−10804.
(55) Woutersen, S.; Mu, Y.; Stock, G.; Hamm, P. *Chem. Phys.* **2001**, *266*, 137−147.
(56) Bagchi, S.; Sam Kim, Y.; Charnley, A. K.; Smith, A. B., III; Hochstrasser, R. M. *J. Phys. Chem. B* **2007**, *111*, 3010−3018.
(57) Eom, I.; Joo, T. *J. Chem. Phys.* **2009**, *131*, 244507.
(58) Jimenez, R.; Fleming, G. R.; Kumar, P. V.; Maroncelli, M. *Nature* **1994**, *369*, 471−473.
(59) Maroncelli, M. *J. Chem. Phys.* **1991**, *94*, 2084−2103.
(60) Rosenthal, S. J.; Xie, X.; Du, M.; Fleming, G. R. *J. Chem. Phys.* **1991**, *95*, 4715−4718.
(61) Zhao, L.; Lustres, L. P.; Farztdinov, V.; Ernsting, N. P. *Phys. Chem. Chem. Phys.* **2005**, *7*, 1716−1725.
(62) Fonseca, T.; Ladanyi, B. M. *J. Phys. Chem.* **1991**, *95*, 2116−2119.
(63) Kumar, P. V.; Maroncelli, M. *J. Chem. Phys.* **1995**, *103*, 3038−3060.
(64) Beneducci, A. *J. Mol. Liq.* **2008**, *138*, 55−60.
(65) Maroncelli, M.; Fleming, G. R. *J. Chem. Phys.* **1987**, *86*, 6221−6239.
(66) Steinel, T.; Asbury, J. B.; Zheng, J.; Fayer, M. D. *J. Phys. Chem. A* **2004**, *108*, 10957−10964.
(67) Nicodemus, R. A.; Ramasesha, K.; Roberts, S. T.; Tokmakoff, A. *J. Phys. Chem. Lett.* **2010**, *1*, 1068−1072.
(68) Lock, A. J.; Woutersen, S.; Bakker, H. J. *J. Phys. Chem. A* **2001**, *105*, 1238−1243.
(69) Gaffney, K. J.; Davis, P. H.; Piletic, I. R.; Levinger, N. E.; Fayer, M. D. *J. Phys. Chem. A* **2002**, *106*, 12012−12023.
(70) Samant, V.; Singh, A. K.; Ramakrishna, G.; Ghosh, H. N.; Ghanty, T. K.; Palit, D. K. *J. Phys. Chem. A* **2005**, *109*, 8693−8704.
(71) Mondal, J. A.; Samant, V.; Varne, M.; Singh, A. K.; Ghanty, T. K.; Ghosh, H. N.; Palit, D. K. *ChemPhysChem* **2009**, *10*, 2995−3012.
(72) Pham, V.-T.; Penfold, T. J.; van der Veen, R. M.; Lima, F.; El Nahhas, A.; Johnson, S. L.; Beaud, P.; Abela, R.; Bressler, C.; Tavernelli, I.; Milne, C. J.; Chergui, M. *J. Am. Chem. Soc.* **2011**, *133*, 12740−12748.
(73) Bräm, O.; Penfold, T. J.; Cannizzo, A.; Chergui, M. *Phys. Chem. Chem. Phys.* **2012**, *14*, 3513−3519.
(74) Zgrablić, G.; Haacke, S.; Chergui, M. *J. Phys. Chem. B* **2009**, *113*, 4384−4393.
(75) Zgrablić, G.; Voitchovsky, K.; Kindermann, M.; Haacke, S.; Chergui, M. *Biophys. J.* **2005**, *88*, 2779−2788.
(76) Bräm, O.; Messina, F.; El-Zohry, A. M.; Cannizzo, A.; Chergui, M. *Chem. Phys.* **2012**, *393*, 51−57.
(77) Barbara, P. F.; Walker, G. C.; Kang, T. J.; Jarzeba, W. *Proc. SPIE* **1990**, *1209*, 18−31.
(78) Shirota, H.; Pal, H.; Tominaga, K.; Yoshihara, K. *J. Phys. Chem.* **1996**, *100*, 14575−14577.
(79) Lee, S.-H.; Lee, J.-H.; Joo, T. *J. Chem. Phys.* **1999**, *110*, 10969−10977.
(80) Pant, D.; Levinger, N. E. *J. Phys. Chem.* **1999**, *103*, 7846−7852.